Energy Advances

ROYAL SOCIETY OF CHEMISTRY

COMMUNICATION

View Article Online
View Journal | View Issue

Cite this: *Energy Adv.*, 2022, 1, 62

Received 29th November 2021,
Accepted 18th December 2021

DOI: 10.1039/d1ya00068c

rsc.li/energy-advances

Stabilizing all-inorganic $CsPbI_3$ perovskite films with polyacrylonitrile for photovoltaic solar cells†

Guanghui Yu,[ab] Ke-Jian Jiang,*[b] Wei-Min Gu,[bc] Yue Zhang,[b] Yanting Xu,[b] Tangyue Xue,[ab] Xinning Jiao,[b] Yiqiang Zhang*[a] and Yanlin Song*[b]

A solution-processed $CsPbI_3$ perovskite film usually suffers from nonuniform crystallization owing to its inorganic components, leading to its poor surface morphology and various defects on the surface and grain boundaries. Herein, polyacrylonitrile (PAN) was employed as a defect passivator for $CsPbI_3$ perovskite films. The nitrile (C≡N) groups on the side chains of the PAN chain skeleton could passivate an undercoordinated Pb ion with a partial positive charge by donating their lone pair of electrons from the N atom, decreasing the density of defect states and enhancing the energy barrier of phase transition. In addition, the incorporation of PAN triggered the nucleation of the perovskite precursor, leading to the formation of a dense $CsPbI_3$ perovskite film with high coverage. Moreover, the robust PAN in the perovskite film enhanced the thermal and water resistance properties of the perovskite film. As a result, the unencapsulated $CsPbI_3$ perovskite cells exhibited superior thermal and humidity stability with 16.21% power conversion efficiency. This work provides a liable polymer passivator to further improve both the efficiency and stability of $CsPbI_3$-based solar cells.

Introduction

Organic–inorganic hybrid perovskites have attracted tremendous attention because of their excellent optoelectronic properties and low-temperature solution-processing ability.[1–4] The power conversion efficiency (PCE) of solution processed perovskite solar cells (PSCs) has increased from an initial 3.8% to a certified 25.5%.[1,3] Although continuous progress in improving efficiency has been made in organic–inorganic hybrid perovskites, the long-term stability issue from the degradation and volatilization of organic groups, *e.g.*, methylammonium (MA^+) and formamidinium (FA^+) cations, is still one of the key challenges for their practical applications. Replacing the organic cations with Cs^+ ions for all-inorganic perovskites, especially $CsPbI_3$ with a suitable optical bandgap (≈1.7 eV), has attracted intense research attention recently because of their intrinsic chemical stability. However, $CsPbI_3$ suffers from a serious phase stability problem; photoactive black-phase $CsPbI_3$ tends to convert into a non-perovskite yellow phase (δ-$CsPbI_3$) under thermal or humid stress.[5–8] In 2014, Choi *et al.* first reported $CsPbI_3$-based PSCs. However, the PCE is very low (0.09%) due to the presence of nonperovskite δ-$CsPbI_3$ in the devices.[5] Thereafter, various methods were developed to stabilize the black $CsPbI_3$ phase at room temperature *via* distortion of PbI_6 octahedra without breaking the three-dimensional (3D) Pb–I network. Swarnkar *et al.* utilized stable cubic-phase $CsPbI_3$ perovskite quantum dots (QDs) to fabricate photovoltaic devices with a PCE of 10.77%.[6] Wang *et al.* developed a solvent controlled growth method to prepare a $CsPbI_3$ film, and the resultant solar cell showed a PCE of 15.7% in a N_2-filled glovebox.[7] In 2015, Eperon *et al.* introduced hydroiodic acid (HI) into $CsPbI_3$ precursor solution in *N*,*N*-dimethylformamide (DMF) to stabilize the black perovskite phase at room temperature.[8] Recently, great efforts have been devoted to the fabrication of HI-related $CsPbI_3$ films, and the device exhibited high PCEs of ~20% with enhanced stability. It has been known that the introduction of dimethylammonium iodide (DMAI), generated through the reaction between HI and DMF, plays a key role in tuning the intermediate phase and crystallization processes of the $CsPbI_3$ film.[9–20] Moreover, defect passivation is found to be another effective method for further improvement of both the efficiency and stability of $CsPbI_3$ solar cells.[18–28]

In the past years, small-molecule organic ammonium salts have been employed to passivate the defects in $CsPbI_3$ films.[18–20] Zhao *et al.* introduced phenyltrimethylammonium chloride (PTACl) to passivate the defects at the surfaces and grain boundaries of $CsPbI_3$ films by a solution post-treatment method, and the charge-carrier lifetime of the device was

[a] College of Chemistry, Zhengzhou University, Zhengzhou, 450001, P. R. China. E-mail: yqzhang@zzu.edu.cn
[b] Key Laboratory of Green Printing, Institute of Chemistry, CAS, Beijing, 100190, P. R. China. E-mail: ylsong@iccas.ac.cn, kjjiang@iccas.ac.cn
[c] School of Chemical Science, University of Chinese Academy of Sciences, Beijing, 100049, P. R. China

† Electronic supplementary information (ESI) available. See DOI: 10.1039/d1ya00068c

greatly increased with a PCE of up to 19%.[18] Recently, the Seok group achieved a high PCE of up to 20.37% through surface-defect passivation of $CsPbI_3$ films using octylammonium iodide.[19] Different from the surface passivation reported above, bulk defect passivation was developed by the Meng group, where a urea-ammonium thiocyanate (UAT) molten salt was directly introduced into $CsPbI_3$ precursor solution. It was found that SCN^- anions could be fully released from UAT and strongly coordinate with the Pb–I octahedron, improving the $CsPbI_3$ film morphology and significantly suppressing the defects and the non-radiative charge recombination of the film. With the optimal UAT component, the $CsPbI_3$ solar cell exhibited a high efficiency of over 20.0%.[20] However, the high diffusion coefficient and strong volatility of such organic small-molecule passivation agents could weaken the passivation effect and the thermal stability of PSCs. Thus, polymer passivation agents with the same functional groups are expected to overcome these shortcomings.[21–25] Previously, Li *et al.* introduced poly(4-vinylpyridine) (PVP) as a passivation agent to synthesize long-term stable cubic $CsPbI_3$.[21] The acylamino groups in PVP enhanced the electron cloud density on the surface of $CsPbI_3$, thus reducing the surface energy. The resultant device showed excellent thermal/moisture stability, but a low PCE of 10.7%. In addition, Wei *et al.* introduced a PMMA (poly(methyl methacrylate)) buffer layer in $CsPbI_3$-based solar cells to passivate interface defects, and suppress defect state-induced carrier recombination. The devices with PMMA showed enhanced stability with a PCE of 10.99%.[23] Recently, Yang *et al.* employed poly(styrene-*co*-acrylonitrile) polymer (PS-PAN polymer) to modify the surfaces of organic–inorganic hybrid perovskite films.[25] The nitrile (C≡N) groups in the side chain could coordinate with Pb^{2+} defects at the surface and the grain boundaries of the perovskite, similar to CN-containing small molecules reported previouly.[25–28]

In this work, polyacrylonitrile (PAN) was employed as a passivation agent to passivate bulk $CsPbI_3$ perovskite defects and improve the device stability. It was found that the nitrile (C≡N) groups in the side chain could coordinate with Pb^{2+} defects at the surface and the grain boundaries. In addition, the incorporation of PAN could trigger the nucleation of the perovskite precursor, leading to the formation of a denser $CsPbI_3$ perovskite film with high coverage. Moreover, the robust PAN in the perovskite films effectively enhanced the thermal and water resistance properties of the perovskite film. As a result, the PAN modified $CsPbI_3$ solar cells exhibited a high PCE of 16.21% with significantly enhanced stabilities.

Results and discussion

Polyacrylonitrile (PAN) was commercially available with average M_w 50 000, where the functional nitrile groups (C≡N) are attached on the side chains of the C–C chain skeleton (Fig. S1, ESI†). It exhibits high thermal stability with a decomposition temperature of up to 300 °C, much higher than the processing temperatures (~200 °C) of the $CsPbI_3$ films,

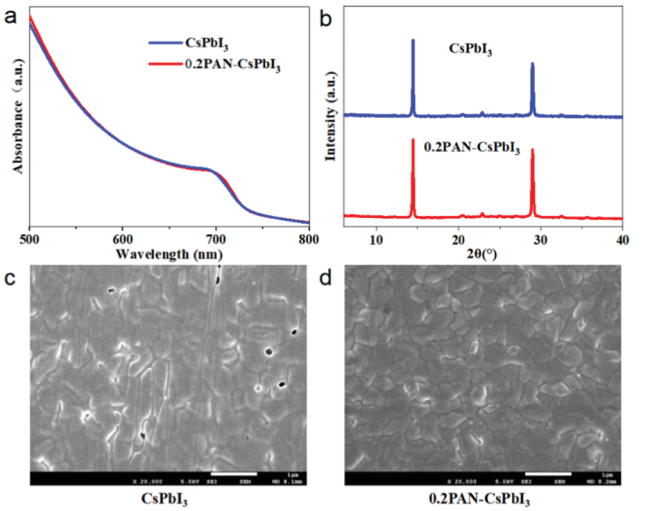

Fig. 1 UV-vis (a) and XRD (b) spectra of $CsPbI_3$ and 0.2PAN–$CsPbI_3$ thin films, and top-surface SEM images of $CsPbI_3$ (c) and 0.2PAN–$CsPbI_3$ films (d). Scale bar, 1 μm.

ensuring that the PAN remains in the $CsPbI_3$ films after the processing (Fig. S2, ESI†).

$CsPbI_3$ perovskite thin films were fabricated by the one-step spin coating method reported by Wang *et al.*,[18] where the precursor solution is composed of stoichiometric cesium iodide (CsI), lead iodide (PbI_2), and dimethylammonium iodide (DMAI) in DMF with a concentration of 0.6 M. For a PAN-modified film, a certain amount of PAN was added to the solution. The resulting film is denoted as *x*PAN–$CsPbI_3$ (*x*: the mass percent of PAN to $CsPbI_3$). Fig. 1a and Fig. S3 (ESI†) show the ultraviolet-visible (UV-vis) absorption spectra of the *x*PAN–$CsPbI_3$ films (*x*: 0–0.3). It was found that all the films showed the same absorption properties with the absorption edge at ~736 nm, corresponding to band gaps of about 1.68 eV (Fig. S4, ESI†). The result indicated that the incorporation of PAN did not affect light absorption of the resultant films. In addition, the X-ray diffraction (XRD) patterns (Fig. 1b and Fig. S5, ESI†) showed that all the films exhibited the same diffraction peaks, indicating that the PAN did not enter into the perovskite crystal, but remained at the surface and grain boundaries of the perovskite films. Fig. 1c and d and Fig. S6 (ESI†) show the scanning electron microscopy (SEM) images of the *x*PAN–$CsPbI_3$ films. It could be observed that the control film without PAN exhibited a poor morphology with a lot of pin holes, probably due to the fast crystallization of the inorganic perovskite commonly observed previously.[29–34] In addition, the removal of a large amount of DMAI from the films at high temperature could contribute to the formation of pinholes. It was observed that the pinhole density decreased with the addition of PAN, and almost disappeared when the *x* was increased to 0.2 (0.2PAN-$CsPbI_3$ film). However, the pinhole density increased with the further addition of PAN ($x = 0.3$) in the films. This result indicates that the appropriate amount of PAN would favour the nucleation and crystal growth of the perovskite for the formation of pin hole-free $CsPbI_3$ films.[35]

To confirm the existence of PAN and the interaction with $CsPbI_3$ in the films, Fourier transform infrared spectroscopy (FTIR) measurement was performed. As shown in Fig. 2a, and Fig. S7 (ESI†), pure PAN exhibited absorption bands in the regions of 2941 cm^{-1} and 2247 cm^{-1}, which were attributed to the functional C–H and C≡N in PAN, respectively. To check the interaction between PAN and $CsPbI_3$, excess PAN was incorporated in $CsPbI_3$ (PAN : $CsPbI_3$, 1 : 100, by wt) for FTIR. It was found that the two characteristic vibrations of PAN were blue-shifted to 2931 cm^{-1} for the C–H stretching, and 2243 cm^{-1} for the C≡N stretching, respectively, indicating the interaction between PAN and $CsPbI_3$. In order to investigate the interaction mechanism, solid-state ^{13}C magic angle spinning (MAS) NMR spectroscopy was performed. As shown in Fig. 2b, two broad peaks in the pristine PAN were observed at 30.1 and 121.6 ppm, which were ascribed to the main chain C–C and C≡N groups, respectively, and well consistent with a previous report.[36] After the incorporation of PAN in the $CsPbI_3$ film, the C signals were shifted to 29.3 ppm for the C–C group and 122.4 ppm for the C≡N group, further demonstrating the chemical action between the PAN and the perovskite. To further confirm the interaction between the PAN and the perovskite film, X-ray photoelectron spectroscopy (XPS) was performed to study the chemical states of the samples. As shown in Fig. 2c, two main peaks for the Pb4f were located at 143.20 eV for Pb $4f_{5/2}$ and 138.30 eV for Pb $4f_{7/2}$ in the pristine perovskite film. After the incorporation of PAN, both the peaks were shifted towards low binding energies of 143.05 and 138.15 eV, respectively, suggesting an increased electron cloud density on Pb from the N lone pair electrons in the C≡N group. In addition, the N 1s peak from the C≡N group observed at 399.6 eV in the neat PAN was shifted to 400.1 eV after the PAN incorporation (Fig. 2d), indicating decreased electron density near the N in the C≡N group, consistent with the binding energy change from the Pb 4f.

Ultra-violet photoelectron spectra (UPS) were recorded for $CsPbI_3$ films with and without PAN, as shown in Fig. 3a and b. The valence and conduction bands of 0.2PAN–$CsPbI_3$ were found to be slightly up-shifted as compared those of the pristine $CsPbI_3$ according to the UPS and the Tauc plots shown in Fig. S8 and S9 (ESI†). The shift could help carrier extraction at the interface between the $CsPbI_3$ and Spiro-OMeTAD hole transport material, contributing to an enhanced open-circuit voltage (V_{OC}) in the devices. To further investigate the effect of PAN on the electronic properties of the perovskite film, steady-state photoluminescence (PL) and time-resolved photoluminescence (TRPL) measurements were performed. As shown in Fig. 3c, the 0.2PAN–$CsPbI_3$ film exhibited a slower decay behaviour than the pristine film. Both the curves could be fit to a biexponential function, giving a fast time constant τ_1 (corresponding to the fast nonradiative recombination induced by defects or impurities) and a slow time constant τ_2 (representing the radiative recombination of the charge carriers in the bulk). The τ_{ave} value was found to increase from 3.42 to 6.93 ns after the incorporation of PAN in the 0.2PAN–$CsPbI_3$ film. In addition, the PL intensity was increased about 3 times after the PAN inclusion (Fig. 3d), which was consistent with the TRPL result. The results indicate lower defect density in the 0.2PAN–$CsPbI_3$ film, which mainly originates from the efficient passivation effect due to the PAN.

It is known that black β-$CsPbI_3$ is unstable thermodynamically, and could be converted to δ-$CsPbI_3$ at room temperature, especially in a humid environment. With the inclusion of PAN polymer on the surface and the grain boundaries, the resulting film resistance to the moisture could be enhanced to improve the stability of the black β-$CsPbI_3$. To check the role of PAN in the $CsPbI_3$ stability, perovskite films without and with PAN (x = 0.2) were fabricated on glass substrates, and stored under

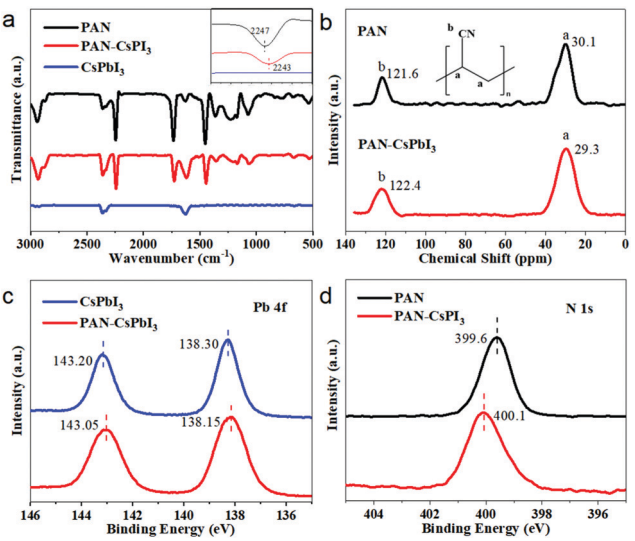

Fig. 2 (a) FTIR spectra of PAN, PAN–$CsPbI_3$, and the $CsPbI_3$. (b) ^{13}C NMR spectra of PAN and PAN–$CsPbI_3$. (c) Pb 4f and (d) N 1s XPS spectra of PAN and PAN–$CsPbI_3$.

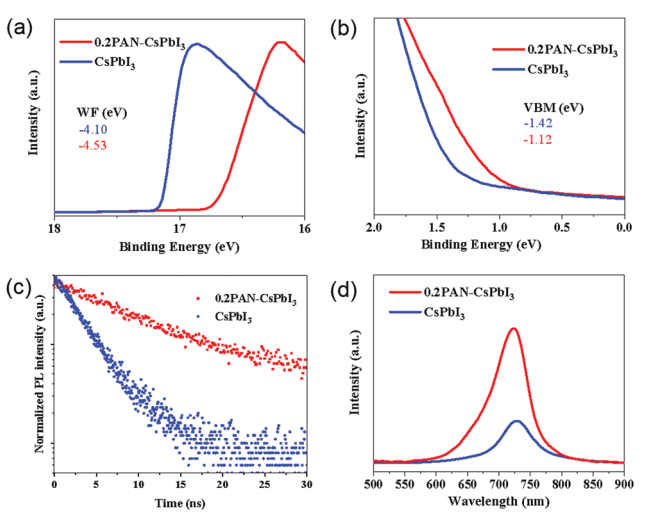

Fig. 3 UPS (a and b), TRPL (c) and PL (d) spectra of the pristine $CsPbI_3$ and 0.2PAN–$CsPbI_3$ films.

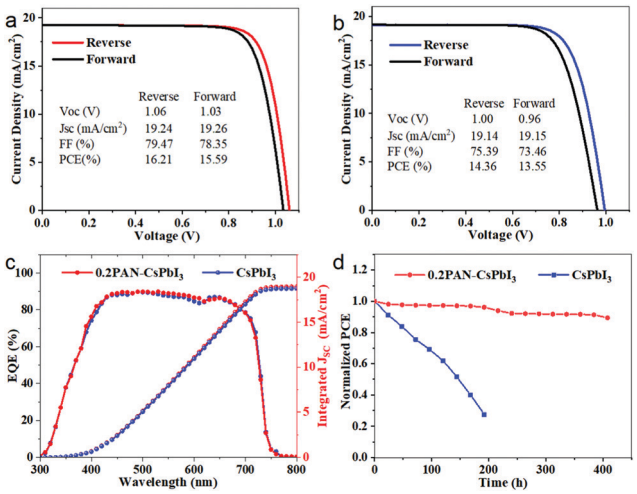

Fig. 4 Current density–voltage (*J*–*V*) characteristics of the (a) control and (b) target devices. (c) EQE and integrated curves of the control and target devices. (d) Environmental stability of the control and target devices (unencapsulated in air at 25 °C and 20–30% relative humidity).

ambient conditions with 30 ± 5% RH and at 25 ± 5 °C for the stability test. As shown in the XRD spectra in Fig. S10 (ESI†), a significant diffraction peak at 9.9° emerged in the control film after 24 h aging, indicating the formation of yellow δ-$CsPbI_3$.[37] In contrast, the target sample retained the original diffraction patterns under the same conditions. In addition, the high stability of the 0.2PAN–$CsPbI_3$ film was also confirmed by the UV-vis absorption spectra shown in Fig. S11 (ESI†).

To verify the effect of the PAN inclusion in the $CsPbI_3$ layer on the photovoltaic performance of PSCs, we prepared solar cells with a glass/fluorine doped tin oxide (FTO)/TiO_2/*x*PAN–$CsPbI_3$/Spiro-OMeTAD/Au configuration, where the $CsPbI_3$ perovskite films were fabricated by the one-step spin coating method reported previously,[18] and the *x* value is 0 and 0.2 for the control device and the target device, respectively. Fig. 4a and b show the optimized current density (*J*)–voltage (*V*) curves of the control and target devices, respectively, measured under both reverse and forward scans (the scan rate is 0.1 V s^{-1}) under 100 mW cm^{-2} AM1.5G illumination. The corresponding PV performance parameters are listed in the figures. The control device without PAN showed a PCE of 14.36 (13.55)% with a fill factor (FF) of 75.39 (73.46)%, a short-circuit current (J_{sc}) of 19.14 (19.15) mA cm^{-2}, and an open-circuit voltage (V_{OC}) of 1.00 (0.96) V in the reverse (forward) scan. In contrast, the target device with PAN exhibited a higher PCE of 16.21 (15.59)% with a FF of 79.47 (78.35)%, a J_{sc} of 19.24 (19.26) mA cm^{-2} and a V_{OC} of 1.06 (1.03) V under the same conditions. The integrated J_{sc} values obtained from the external quantum efficiency (EQE) spectra matched well with the *J*–*V* measured values (Fig. 4c). The increase in PCE for the target device is mainly due to the improved V_{OC} and FF, suggesting a satisfactory passivation effect from the PAN.[18–20] The stability of the unencapsulated devices was preliminarily tested in air at 25 °C and 20–30% relative humidity. As shown in Fig. 4d, the control device lost 72% of its initial PCE after 200 h aging, while the target device still retained 89% of its initial PCE after 400 h aging. The result clearly indicates that the incorporation of PAN can enhance both the efficiency and stability of the photovoltaic solar cells.

Conclusion

In summary, polyacrylonitrile (PAN) was employed for the fabrication of all-inorganic $CsPbI_3$ perovskite films. It was found that the nitrile group in PAN could passivate the defects on the surface and grain boundaries of the $CsPbI_3$ perovskite films. In addition, the PAN assisted the nucleation and the crystal growth for the formation of pinhole-free $CsPbI_3$ perovskite films. Moreover, the polymer properties of PAN can enhance the thermal and humidity stability of the $CsPbI_3$ film. With the optimization of PAN in the perovskite film, the efficiency of the device was increased by about 13% compared with the control samples. Moreover, the device stability was significantly enhanced under ambient conditions. This result provides an effective and robust approach for the fabrication of all-inorganic $CsPbI_3$ perovskite solar cells.

Conflicts of interest

There are no conflicts to declare.

Acknowledgements

This work was supported by the National Key R&D Program of China (Grant No. 2018YFA0208501), the National Natural Science Foundation of China (Grant No. 51803217, 51773206, 61874123, 91963212, 21401167), the External Cooperation Program of Chinese Academy of Sciences (Grant No. GJHZ201948) and the Key R&D and Promotion Project of Henan Province (Grant No. 192102210032). The authors also thank the Advanced Analysis & Computation Center at Zhengzhou University for materials and device characterization support.

Notes and references

1 A. Kojima, K. Teshima, Y. Shirai and T. Miyasaka, *J. Am. Chem. Soc.*, 2009, **131**, 6050–6051.
2 P. Li, Y. Zhang, C. Liang, G. Xing, X. Liu, F. Li, X. Liu, X. Hu, G. Shao and Y. Song, *Adv. Mater.*, 2018, **30**, 1805323.
3 National Renewable Energy Laboratory (NREL), Best Research-Cell Efficiencies Chart, https://www.nrel.gov/pv/cell-efficiency.html.
4 J. Jeong, M. Kim, J. Seo, H. Lu, P. Ahlawat, A. Mishra, Y. Yang, M. A. Hope, F. T. Eickemeyer, M. Kim, Y. J. Yoon, I. W. Choi, B. P. Darwich, S. J. Choi, Y. Jo, J. H. Lee, B. Walker, S. M. Zakeeruddin, L. Emsley, U. Rothlisberger, A. Hagfeldt, D. S. Kim, M. Grätzel and J. Y. Kim, *Nature*, 2021, **592**, 381–385.
5 H. Choi, J. Jeong, H.-B. Kim, S. Kim, B. Walker, G.-H. Kim and J. Y. Kim, *Nano Energy*, 2014, **7**, 80–85.

6 A. Swarnkar, A. R. Marshall, E. M. Sanehira, B. D. Chernomordik, D. T. Moore, J. A. Christians, T. Chakrabarti and J. M. Luther, *Science*, 2016, **354**, 92–95.
7 P. Wang, X. Zhang, Y. Zhou, Q. Jiang, Q. Ye, Z. Chu, X. Li, X. Yang, Z. Yin and J. You, *Nat. Commun.*, 2018, **9**, 2225.
8 G. E. Eperon, G. M. Paternò, R. J. Sutton, A. Zampetti, A. A. Haghighirad, F. Cacialli and H. J. Snaith, *J. Mater. Chem. A*, 2015, **3**, 19688–19695.
9 P. Luo, W. Xia, S. Zhou, L. Sun, J. Cheng, C. Xu and Y. Lu, *J. Phys. Chem. Lett.*, 2016, **7**, 3603–3608.
10 Y. Jiang, J. Yuan, Y. Ni, J. Yang, Y. Wang, T. Jiu, M. Yuan and J. Chen, *Joule*, 2018, **2**, 1356–1368.
11 F. Li, Y. Pei, F. Xiao, T. Zeng, Z. Yang, J. Xu, J. Sun, B. Peng and M. Liu, *Nanoscale*, 2018, **10**, 6318–6322.
12 B. Zhao, S.-F. Jin, S. Huang, N. Liu, J.-Y. Ma, D.-J. Xue, Q. Han, J. Ding, Q.-Q. Ge, Y. Feng and J.-S. Hu, *J. Am. Chem. Soc.*, 2018, **140**, 11716–11725.
13 Y. Wang, T. Zhang, F. Xu, Y. Li and Y. Zhao, *Sol. RRL*, 2018, **2**, 1700180.
14 Y. Wang, M. I. Dar, L. K. Ono, T. Zhang, M. Kan, Y. Li, L. Zhang, X. Wang, Y. Yang, X. Gao, Y. Qi, M. Grätzel and Y. Zhao, *Science*, 2019, **365**, 591–595.
15 H. Bian, H. Wang, Z. Li, F. Zhou, Y. Xu, H. Zhang, Q. Wang, L. Ding, S. Liu and Z. Jin, *Adv. Sci.*, 2020, **7**, 1902868.
16 W. Ke, I. Spanopoulos, C. C. Stoumpos and M. G. Kanatzidis, *Nat. Commun.*, 2018, **9**, 4785.
17 H. Meng, Z. Shao, L. Wang, Z. Li, R. Liu, Y. Fan, G. Cui and S. Pang, *ACS Energy Lett.*, 2020, **5**, 263–270.
18 Y. Wang, Xi Liu, T. Zhang, X. Wang, M. Kan, J. Shi and Y. Zhao, *Angew. Chem., Int. Ed.*, 2019, **58**, 16691–16696.
19 S. M. Yoon, H. Min, J. B. Kim, G. Kim, K. S. Lee and S. Seok II, *Joule*, 2021, **5**, 183–196.
20 B. Yu, J. Shi, S. Tan, Y. Cui, W. Zhao, H. Wu, Y. Luo, D. Li and Q. Meng, *Angew. Chem., Int. Ed.*, 2021, **60**, 13436–13443.
21 B. Li, Y. Zhang, L. Fu, T. Yu, S. Zhou, L. Zhang and L. Yin, *Nat. Commun.*, 2018, **9**, 1076.
22 R. Saraf and V. Maheshwari, *ACS Appl. Energy Mater.*, 2019, **2**, 2214–2222.
23 W. Wei, W. Chen, X. Zhao, Z. Yang and Y. Liu, *J. Alloys Compd.*, 2021, **891**, 161985.
24 Z. Huang, X. Hu, C. Liu, L. Tan and Y. Chen, *Adv. Funct. Mater.*, 2017, **27**, 1703061.
25 J. Yang, Q. Cao, Z. He, X. Pu, T. Li, B. Gao and X. Li, *Nano Energy*, 2021, **82**, 105731.
26 T. Wu, Y. Wang, Z. Dai, D. Cui, T. Wang, X. Meng, E. Bi, X. Yang and L. Han, *Adv. Mater.*, 2019, **31**, 1900605.
27 Y. Lin, L. Shen, J. Dai, Y. Deng, Y. Wu, Y. Bai, X. Zheng, J. Wang, Y. Fang, H. Wei, W. Ma, X. C. Zeng, X. Zhan and J. Huang, *Adv. Mater.*, 2017, **29**, 1604545.
28 J. Wang, J. Zhang, Y. Zhou, H. Liu, Q. Xue, X. Li, C.-C. Chueh, H.-L. Yip, Z. Zhu and A. K. Y. Jen, *Nat. Commun.*, 2020, **11**, 177.
29 T. Zhang, M. I. Dar, G. Li, F. Xu, N. Guo, M. Grätzel and Y. Zhao, *Sci. Adv.*, 2017, **3**, e1700841.
30 Y. Wang, T. Zhang, M. Kan and Y. Zhao, *J. Am. Chem. Soc.*, 2018, **140**, 12345–12348.
31 X. Ding, M. Cai, X. Liu, Y. Ding, X. Liu, Y. Wu, T. Hayat, A. Alsaedi and S. Dai, *ACS Appl. Mater. Interfaces*, 2019, **11**, 37720–37725.
32 Y. Wang, G. Chen, D. Ouyang, X. He, C. Li, R. Ma, W.-J. Yin and W. C. H. Choy, *Adv. Mater.*, 2020, **32**, 2000186.
33 S. Fu, L. Wan, W. Zhang, X. Li, W. Song and J. Fang, *ACS Energy Lett.*, 2020, **5**, 3314–3321.
34 T. Moot, A. R. Marshall, L. M. Wheeler, S. N. Habisreutinger, T. H. Schloemer, C. C. Boyd, D. R. Dikova, G. F. Pach, A. Hazarika, M. D. McGehee, H. J. Snaith and J. M. Luther, *Adv. Energy Mater.*, 2020, **10**, 1903365.
35 D. Bi, C. Yi, J. Luo, J.-D. Décoppet, F. Zhang, S. M. Zakeeruddin, X. Li, A. Hagfeldt and M. Grätzel, *Nat. Energy*, 2016, **1**, 16142.
36 Y. H. Choi, C. M. Choi, D. H. Choi, Y. Paik, B. J. Park, Y. K. Joo and N. J. Kim, *J. Membr. Sci.*, 2011, **371**, 84–89.
37 J. Zhang, J. Liu, A. Tan, J. Piao and Z. Fu, *Chem. Commun.*, 2020, **56**, 13816–13819.